Influence of spring stiffness and anisotropy on stick-slip atomic force microscopy imaging

Kerssemakers, J.; de Hosson, J. Th. M.

Published in:
Journal of Applied Physics

DOI:
10.1063/1.362870

Influence of spring stiffness and anisotropy on stick-slip atomic force microscopy imaging

J. Kerssemakers and J. Th. M. De Hosson[a)]
Department of Applied Physics, Materials Science Center, University of Groningen, Nijenborgh 4, 9747AG Groningen, The Netherlands

(Received 17 January 1996; accepted for publication 18 March 1996)

This paper presents a detailed analysis of high-load friction atomic force microscopy (AFM) images of layered structures in terms of a discrete stick-slip model. It turned out that based on a geometric approach, the characteristics of slip behavior can be linked to the cantilever/sample spring anisotropy. In particular, the use of polar scans is emphasized to analyze and to quantify these characteristics. The measured stiffness as derived from the slip behavior is in correspondence with the stiffness inferred from static friction. It is concluded that the combined stiffness of substrate and cantilever is constant during an AFM scan in a given direction, which supports the simple stick-slip model. © *1996 American Institute of Physics.* [S0021-8979(96)00814-6]

I. INTRODUCTION

Atomic force microscopy (AFM) is a versatile technique to investigate atomic-scale surface properties. However, the three translational degrees of freedom of the scanning probe often account for an unwanted mix of frictional and topographic information.[1–4] This mixing is influenced by the type of detection that is used and is most prominent with optical lever detection. Another aspect is the influence of the scanning configuration or system itself. The latter concerns cantilever geometry, cantilever mechanical properties, sample orientation, and detector orientation. As far as the detection side is concerned, especially the optical lever system can be shown to be more sensitive to a lateral movement of the probe than a vertical deflection.[5] Keeping this in mind, the interpretation of the detected signal can be rather misleading.

The forces in the perpendicular direction are often associated with the long-axis signal component of the cantilever, while the short-axis component is taken for the friction signal.[6,7] At an atomic scale, one should be cautious in making this assumption: along both axes the scan signal can be shown to follow friction-based behavior, as will be explained later. Even when the origin of the cantilever movement is unambiguously frictional, it is still not straightforward to interpret the signal in terms of the interaction force between probe tip and substrate. In various publications, attention was focused on the strong stick-slip nature of the signal.[4,8–15] Here, the movement of the tip relative to the scan path resembles a relaxation oscillation,[16] i.e., static (stick) phases alternate fast-moving slip-phases. The driving frequency in this picture is the periodicity of the lattice in combination with the scanning speed. Recently, the concept of atomic-periodicity stick slip is made more explicit in a two-dimensional description.[15,17,18] The tip follows the forced scan path of the cantilever base by a series of discrete jumps from lattice point to lattice point. The difference between the continuous cantilever base route and the zig-zag motion of the tip, thus is the predominant cause for the well known images showing atomic resolution, especially of layered compounds (Fig. 1). In literature, this is clarified in various ways that, however, mainly differ in actual representations:

- The perpendicular components of the tip displacement are usually associated with the ''force'' and ''friction'' signal. These signals were used to restore the original route of the tip.[18]
- Simulations of image formation using simple models of the atomic configuration have shown a good resemblance with experimental observation.[15]
- Different signal components were linked to specific slip or jump direction.[16]

Scan signal characteristics, simulations, and scan path reconstruction offer a qualitative way to interpret image formation. To investigate the interaction causing the stick slip in the first place, a more precise way to extract parameters directly from the jumping behavior is needed. In this paper, a procedure is represented that is based on a geometrical approach of the stick-slip system. Since calculations and measurements on cantilevers[19,20] show a certain amount of anisotropy in their lateral stiffness, the jumping behavior is expected to vary with the scan direction. The analysis presented here offers a relatively simple way to quantify the system.

II. DESCRIPTION OF A TWO-DIMENSIONAL STICK-SLIP BEHAVIOR

In a discrete 2D-stick-slip mechanism, only discrete sites are allowed for the tip position. These sites reflect the periodic atomic lattice of the sample surface. The model probe tip is only allowed to jump instantaneously from one site to another, for which a ''jumping criterion'' needs to be defined. The tip displacement is defined as the difference between actual tip position and the fully relaxed tip position, both with the same cantilever base position. The detector will only detect a long-axis projection of this strain. The subsequent displacements and jumps of the tip should follow the forced scan path.

To analyze this jumping behavior, we propose the following coordinate transformation as displayed in Fig. 2. First, the whole system is taken to be two-dimensional in the

a)Electronic mail: hossonj@phys.rug.nl

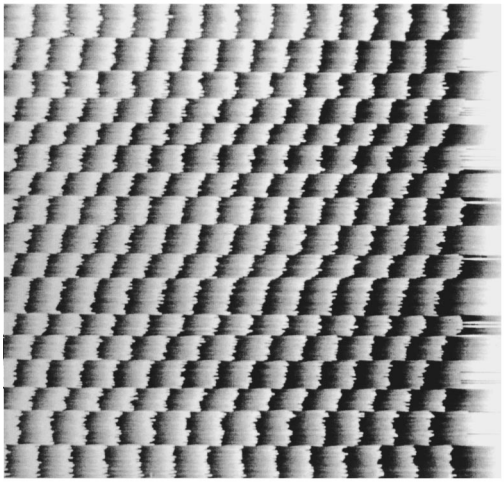

FIG. 1. A $\langle 11\bar{2}0\rangle$ scan on $NbSe_2$. The sharp black-white transitions are a typical feature of stick-slip imaging.

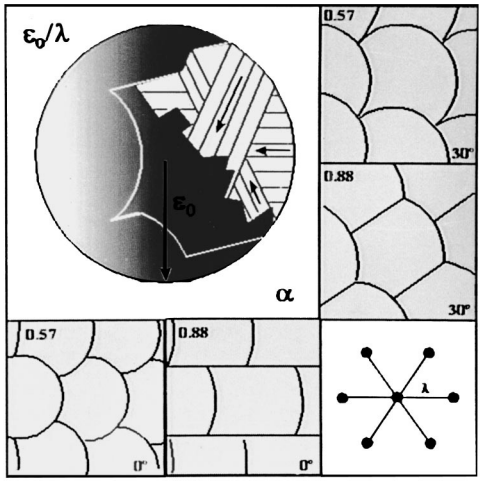

FIG. 3. The stick-slip model predicts atomic unit cell shapes. The contours depend on the ratio ϵ_0/λ (see main text) and the orientation of scanning relative to the lattice.

xy-plane. From the actual displacement opposed to the actual tip and cantilever dimensions, this choice seems to be reasonable. The components (ϵ_x, ϵ_y) represent the two-dimensional displacement vector of the tip. In these coordinates, the stick phase is depicted by a line having the tangent of the relative scan direction α as slope (line A). Each time the displacement magnitude reaches a value ϵ_0, a jump will occur of a lattice translation of length λ. This value roughly corresponds to the better shown ''initial sticking'' value. This translation corresponds to a relaxation and may have only a few possible directions: six for a hexagonal lattice, a symmetry that we will use further on. The maximum-displacement-circle of radius ϵ_0 then can be divided into six parts. Within each part, only one of the six translations is most favorable, giving the strongest relaxation. As a result the actual route of the tip can be seen as a series of straining and relaxing events, all within a circle $r=\epsilon_0$.

The detector signal is proportional to a component of the momentary displacement. The direction of this component depends on the detector-cantilever-laser configuration and is not necessarily along the *x*-axis. In Fig. 2 all possible detector signals form a linear gray value field, through (0,0,0) with one direction of maximum slope (which corresponds to maximum detector sensitivity) and an orthogonal direction of zero slope and sensitivity. In the concept of this model, one can easily construct and subsequently calculate the jump behavior. Also, we may deduce some useful properties as will be explained in the following. For all the mathematical expressions we refer to the appendices.

This model makes sense if each possible λ-jump is truly relaxing. This gives a lower bound on the threshold strain, i.e., $\epsilon_0 \geqslant \lambda/\sqrt{3}$. Below this value, no complete stick-slip behavior can be expected (Appendix A). When a large number of scan and jump routes is followed, the start and end point of a jump form a plane-filling contour. This contour forms exactly the shape of the unit cell emerging in a real AFM image as depicted in Fig. 1. Within the contour, the detector

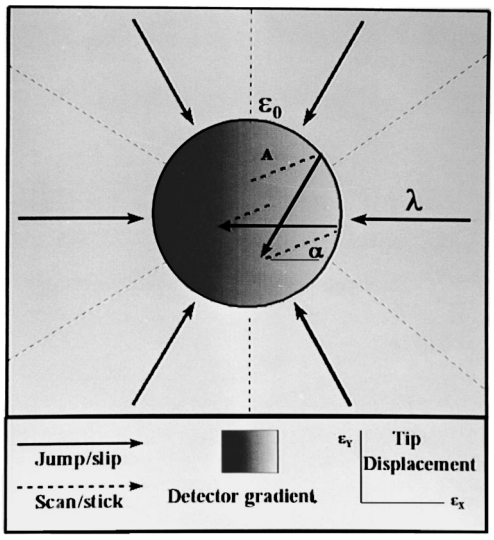

FIG. 2. Stick-slip model. Coordinates (ϵ_x, ϵ_y) represent tip displacement from the (0,0) relaxed position. Possible lattice translations are marked by arrows $A-F$. The shading represents the linear detector signal at any point (ϵ_x, ϵ_y). Jumps occur any time that $|\epsilon|=\epsilon_0$. Any route is described by a sequence of scanning and jumping vector translations.

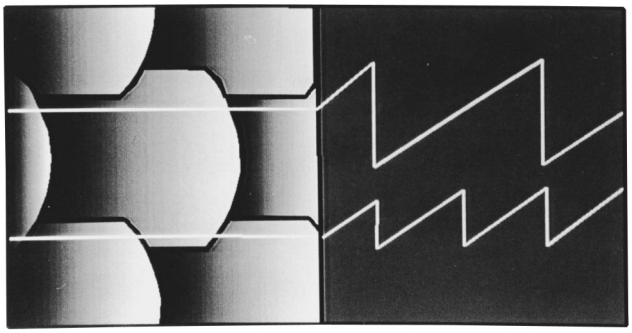

FIG. 4. Zig-zag jump patterns can alternate with straightforward jumping, even at a $\langle 1000\rangle$ direction of scanning. The occurrence of this effect depends on the relative cantilever stiffness.

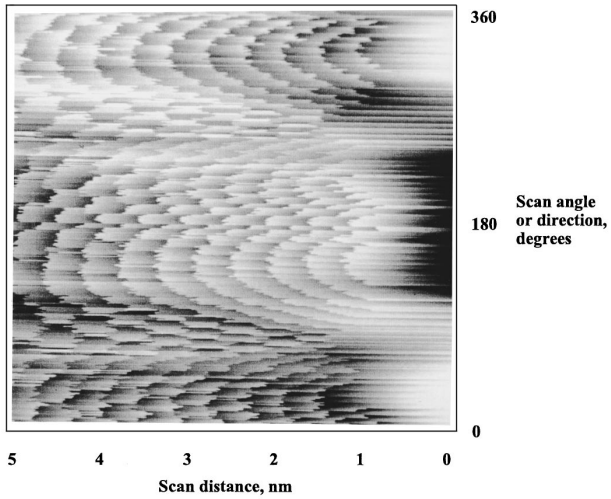

FIG. 5. A polar scan on $NbSe_2$. Each scan line $y=$constant was taken at a different scan angle, from 0 to 360°.

field gray value represents the signal height in the corresponding point in the AFM image. Thus, the appearance of the unit cell is directly shown. Clearly, this appearance depends on the relative orientation of lattice, scan direction, and detector field, together with the ratio ϵ_0/λ. Some examples of possible shapes are shown in Fig. 3. For a given scan angle α, three of the six jump types relax. We call the jump with the direction most parallel to the scan direction the ''straight'' type, while the other two, adjacent to the straight jump at plus and minus 60°, are called ''zig'' and ''zag,'' respectively. All have a length λ. For a long scan route, each jump term will occur a number of times. This number is a specific function of the set $(\alpha,\epsilon_0,\lambda)$ and can be even equal to zero over an interval of α. All jumps together should have their vector sum equal to the linear scan path. Therefore, for long scan routes the relative jump numbers have a constant ratio, and can be normalized to ρ_{zig}, ρ_{straight}, and ρ_{zag}; summing to unity.

Using the model displayed in Fig. 2, these jump densities can be constructed and calculated for any scan system. Here, any such system is entirely described by $(\alpha,\epsilon_0,\lambda)$ together with the detector orientation. This is explained and illustrated in detail in Appendix A. Here we will restrict ourselves to the results. The jump densities will differ in two separate regimes of scan angle α. All three types of jumps will occur whenever

$$0 \leqslant \alpha \leqslant \arctan(\sqrt{3}-2\epsilon_0/\lambda). \tag{1}$$

When this is the case, the jump densities ρ are given by

$$\rho_{\text{zig}} = 1-\frac{1}{2}\left(\frac{1-\tan(\alpha)/\sqrt{3}}{1-\epsilon_0/\lambda\sqrt{3}}\right), \tag{2a}$$

$$\rho_{\text{straight}} = \frac{1}{\lambda\sqrt{3}/\epsilon_0-1}, \tag{2b}$$

$$\rho_{\text{zag}} = 1-\frac{1}{2}\left(\frac{1+\tan(\alpha)/\sqrt{3}}{1-\epsilon_0/\lambda\sqrt{3}}\right), \tag{2c}$$

Only two type of jumps make up the scan route when

FIG. 6. A typical forward and backward loop of a $\langle 11\bar{2}0\rangle$ line scan. Some terms used in the main text are defined.

$$\arctan(\sqrt{3}-2\epsilon_0/\lambda) \leqslant \alpha \leqslant 30. \tag{3}$$

In this case, the densities are

$$\rho_{\text{zig}} = \frac{2}{\sqrt{3}/\tan(\alpha)+1}), \tag{4a}$$

$$\rho_{\text{straight}} = \frac{\sqrt{3}/\tan(\alpha)-1}{\sqrt{3}/\tan(\alpha)+1}, \tag{4b}$$

$$\rho_{\text{zag}} = 0. \tag{4c}$$

The calculations only hold within 30°. However, by symmetry reasons the behavior should be the same to the other side of the ''straight'' jump axis. This, together with the hexasymmetry of the system allows us to use the results to the whole 360° scan angle range. Small scan sizes correspond to short scan routes. When only two jump types occur, the tip needs a certain distance to travel at least before the first ''zig'' jump takes place. Close to a lattice pole direction, this distance exceeds the scan size and thus only the ''straight'' type of jump is observed. The regime in which this effect occurs can be approximated (Appendix A) within 5% by

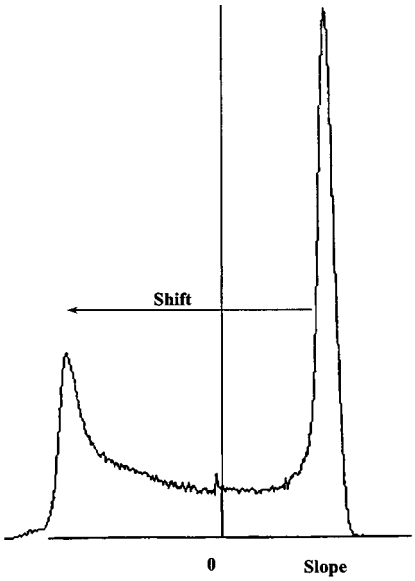

FIG. 7. A slope histogram of a $\langle 1000\rangle$ scan image. Linear regression on a sawtooth signal results in two peaks. The large peak gives the mean upward slope, the small one originates from the steep downward steps.

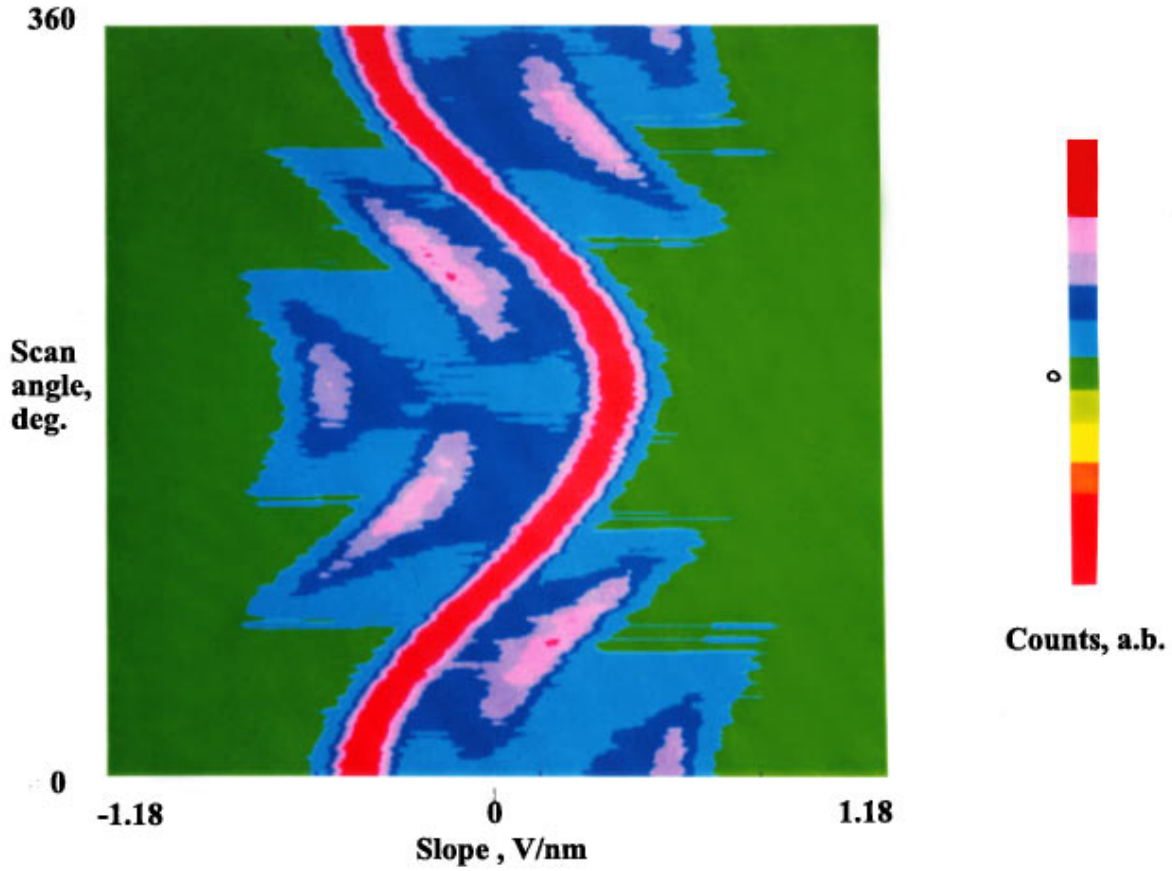

FIG. 8. A two-dimensional slope histogram from a polar AFM image as in Fig. 5. *X* coordinates stand for slope. *Y* coordinates stand for scan angle. Each horizontal line is a slope histogram as in Fig. 7 seen from above. Features in this plot are characteristic for stick-slip images, as is explained.

$$0 \leqslant \alpha \leqslant 60 \frac{(\epsilon_0 - 0.87\lambda)}{\text{scansize}}, \tag{5}$$

for scan size $>10\lambda$ and $\alpha<15$.

The initial sticking can also be measured directly. The distance the tip may travel from a given scan-turning point depends on the displacement at that point. For simplicity, we only consider the shortest possible route. At scanning angles of 0° mod 60, this distance is

$$l_{0 \text{ mod } 60} = \sqrt{3}\epsilon_0 - \lambda. \tag{6}$$

At angles in between, this shortest distance before any jump is slightly larger. In experiments, the situation where three jump types are involved [Eq. (2)] can be recognized easily. Scan routes with mainly ''zig'' and ''zag'' jumps alternate with routes with mainly ''straight'' jumps. At a certain angle, this situation changes in the two-jump type [Eq. (4)]. For $\sqrt{3}/3 \leqslant \epsilon_0/\lambda \leqslant \sqrt{3}/2$, the three jump types situation even persists at $\alpha=0°$, e.g., scanning along a lattice main axis direction. An example of a resulting unit cell is depicted in Fig. 4. This effect has been observed and recognized before.[16] From the optimal-relaxation procedure presented in the model description, we may interpret this zig-zag behavior as being energetically more favorable in the given range of small ϵ_0. The maximum strain is proportional to the ratio of lattice–tip interaction and cantilever stiffness. From Eqs. (1) and (3), the angle α_{zigzag} at which the zig-zag jumping starts is related to ϵ_0 by:

$$\epsilon_0 = \lambda \left[\sqrt{3} - \frac{1}{2} \tan(\alpha_{\text{zigzag}}) \right]. \tag{7}$$

Similarly, the angle α_{zig} where the one-jump situation from Eq. (5) changes in a two jump types case also gives ϵ_0 at that point:

$$\epsilon_0' = \text{scansize}. \frac{\alpha_{\text{zig}}}{60} + 0.87\lambda. \tag{8}$$

For all lattice poles, an ϵ_0 can be measured from the initial sticking l in Eq. (6):

$$\epsilon_0'' = (l + \lambda)/\sqrt{3}. \tag{9}$$

In summary, we can have three stick-slip situations in general, one with only one-jump type involved, one with two-jump types, and one with three. The scan angles at which one situation changes in another are governed by the maximum displacement ϵ_0. These angles and the initial sticking provide from Eqs. (7), (8), and (9) two independent ways to measure this value ϵ_0 for different scan directions.

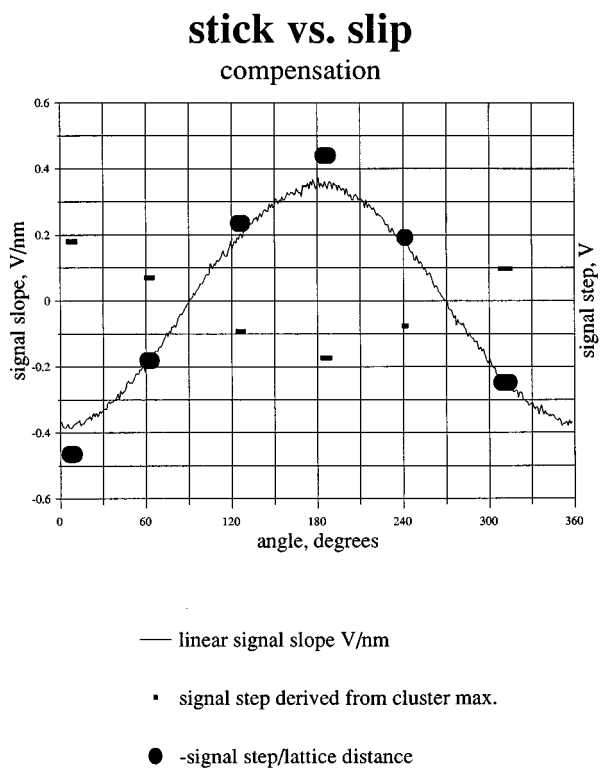

FIG. 9. Along the main lattice directions, pure stick-slip behavior implies that the displacement during stick (resulting in the linear slope) should be completely compensated by an instant jump after each lattice distance. This condition gives a simple means to check whether the system truly behaves like a pure stick-slip system by correlating the cluster maxima from Fig. 8 to the main slope.

When anisotropy is involved, we need to be cautious. The maximum strain circle must be replaced by an ellipse. The $\epsilon_0''(\alpha)$ of Eq. (9) reflects the length of the radius of the displacement ellipse at angle α. The ϵ_0 and ϵ_0' from Eqs. (7) and (8), though, are different. In Appendix A it is clarified that these values correspond to the length of a line segment with both end points on the ellipse. For a circle this length is equal to the radius, but for an ellipse it is not. The angle of this line piece is not parallel but roughly perpendicular to the radius vector at α. If we reconstruct such a maximum displacement ellipse from Eqs. (7), (8), and (9), we need to treat the different ϵ_0's correspondingly to the above. In the following, a comparison with experiments will be made.

III. EXPERIMENTS

We set out to measure the jumping behavior of the tip for different directions on a hexasymmetric lattice. To do this in a compact way, we modified the scan type of a Nanoscope-II optical-lever AFM. The original grid scan was transformed into a polar scan, in which each scan line is scanned at a slightly different orientation, similar to the work of O'Shea.[1] In our work, however, the resulting 400 scan lines are still imaged in 400×400 Cartesian coordinates as shown in Fig. 5. This simplifies angle dependent data processing. In this way, we scanned various materials at ambient atmosphere. We have chosen substrates that were known from their strong stick-slip properties combined with a good probe tip wear resistance, like CdI_2, $NbSe_2$, NbS_2, etc.

To interpret a stick-slip image properly with respect to the above analysis, we need an algorithm that is able to distinguish and count different types of lattice jumps in a given scan line (α). From a single scan line like in Fig. 6 the stick and slip events can be clearly recognized. Furthermore, due to its origin these events possess certain characteristics, namely: I. The detector field (see Fig. 2) is assumed to be linear. When some cantilever deflection is applied along direction α, the sensitivity or slope of the detector signal is proportional to the strain component along the maximum gradient:

$$\text{Slope}=\frac{d(\text{Signal})}{d|\epsilon|}=C.\sin(\alpha-\alpha_o). \tag{10}$$

It implies that the signal will have a constant slope during the stick phase. The magnitude of this slope depends on the scan direction α in a sinusoidal way. In this view, the cantilever is assumed not to buckle sideways. II. Each jump type has a fixed magnitude and direction, independent of the tip displacement (ϵ_x,ϵ_y) at the jump point. It means that each jump will cause a specific step instead of a certain slope. The magnitude of this step is characteristic for the jump type. Along any lattice pole direction, there exists a simple relation between the steps of magnitude Δ and the slope:

$$\Delta=\text{Slope}*\lambda. \tag{11}$$

We can use this relation to check quantitatively whether the actual AFM image is caused by a dynamic system that indeed consists of pure stick and slip phases for all directions.

The ''slope'' and ''step'' characteristics described above point to a logical way of processing: At each image pixel, an N-point linear regression fit was made, and summed in a (slope, counts) histogram. From the former, we expect a large peak at a specific slope S. Furthermore, a step of amplitude Δ will produce a number of shifted values:

$$S_{\text{shift}}-S=\Delta.N/6.x(1-x),\quad x\in\{0,1\},\quad N>8. \tag{12}$$

For the derivation of Eq. (12) we refer to Appendix B. A histogram of this parabolic shape will produce a curve inversely proportional to third-order, peaking sharply at

$$S_{\text{shift}}-S=3\Delta/2N. \tag{13}$$

A simple sawtooth line scan and a corresponding histogram is shown in Figs. 6 and 7. We see the expected large main peak and the sharp secondary jump peak. As the numbers of pixels influenced by a step is only N per jump, the jump peak is relatively small. Following this procedure for each scan line, we obtain a set of (*counts*, *alpha*, *slope*) points. Each single slope count was convoluted with a triangle to make peak detection possible. The result is presented as a two-dimensional contour plot of counts (slope, *alpha*) in Fig. 8. The convolution described earlier causes loss of detail of smaller than ca. 0.15 V/nm along the slope axis. Along the vertical (angle) axis, no smoothing was performed. In Fig. 8, the position at α of the main peak should be given by Eq. (10). In addition we recognize jumps as

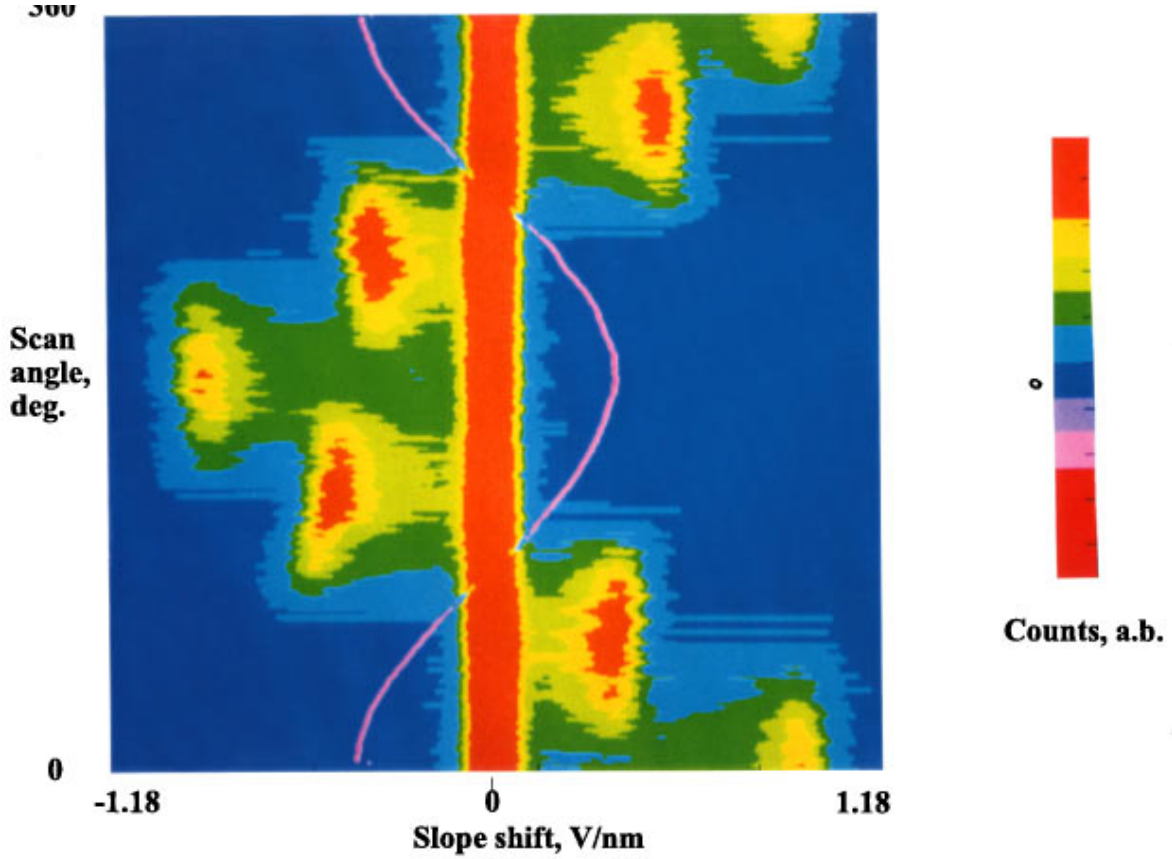

FIG. 10. The two-dimensional slope histogram from Fig. 8, now with the value of the main peak slope subtracted. Six clusters, each with a specific horizontal shift from zero, are originating from the six possible nearest neighbor jumps on a hexagonal lattice. By this substraction, it is now possible to take measured density curves by taking vertical slices through cluster maxima.

clusters with a specific shift from the main peak. This shift is given by Eq. (12). The center position of each cluster corresponds to a lattice pole angle. Along each of these angles, Eq. (11) should hold for the steps and the slope, provided we do have a genuine stick-slip system. This is confirmed in Fig. 9. Here we see the position of the main peak as a curve that fits a sinusoid within 1%. Compared with this curve are the original jump signal steps in mV [calculated with the inverse of Eq. (13)] divided by the lattice distance λ. They coincide reasonably well. Because of this, the system is taken to be purely stick slip, and further analysis of the parameters is appropriate.

In this example, the jump types are clearly divided into six clusters, bounded within definite sectors. The angles at which a cluster ends are α_{zigzag} or α_{zig} and are given by Eqs. (1) or (5), respectively. In Fig. 10, the relative shift of the clusters from the main peak is shown. A cross section along the constant slope axis through the maximum of a cluster shows a curve proportional to the jump density, derived in Eqs. (2) and (4). Both jump densities and cluster slices are shown in Figs. 11 and 12, respectively. Figure 11 shows the densities $\rho(\alpha)$ for different ϵ_0 curves [see Eqs. (2)–(4)].

In Fig. 10, the angles α_{zigzag} or α_{zig} were measured. This should give us a value of the initial sticking ϵ_0 from Eqs. (7) and (8). This value should be considered a rough estimate, as the calculations were all performed for an isotropic system. In this way, the initial sticking was obtained from the jumping behavior. As described earlier, these values should be considered as the length of a line segment with both ends on an ellipsoid. The center of such a line piece was taken along the corresponding lattice pole. Although weak deviations from this are expected when anisotropy is involved, this proves a way to estimate the shape and size of the maximum displacement ellipsoid causing the observed jumping behavior. We can also obtain the shape of this ellipsoid from the raw polar scan with help of Eq. (6). Figure 13 is a polar graph of both values as a function of the scan direction. Although the two different ways of determining the points on the ellipsoid do not produce points at identical directions, the two ellipsoid maps should be the same. Indeed, we observe a correspondence in trend and amplitude, which supports our assumptions.

IV. CONCLUSIONS

We conclude that even complicated zig-zag behavior can be described rather nicely based on geometrical considerations. The only governing physical parameter is the ratio of static friction to system stiffness, the ''initial sticking.'' This implies that, once the state of discrete stick slip occurs, the initial sticking, which can be easily measured at the start of a scan line, is sufficient to predict the characteristics of the

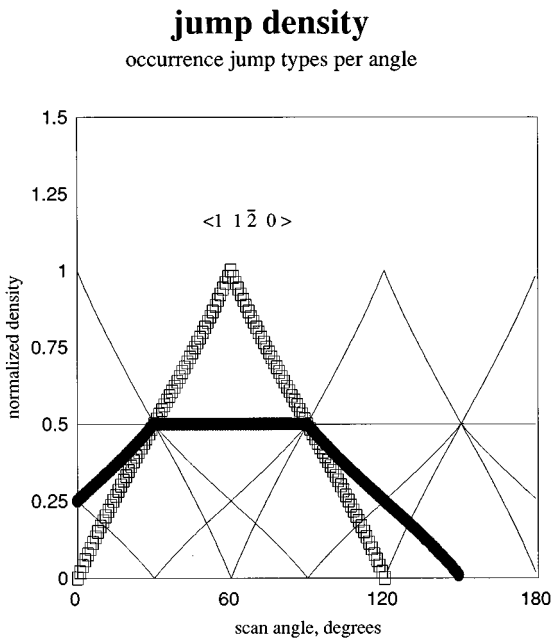

FIG. 11. Theoretical jump density curves as a function of the scan angle. For a given scan direction, the relative occurrence of each of the three relaxing jump types is given as a relative number. For a relatively small maximum cantilever displacement (thick solid line) we see one-jump type extending over a maximal range of 180°, implying zig-zag jump behavior. This range narrows and ultimately becomes independent of the maximum displacement when the latter exceeds 0.88 times the nearest-neighbor distance. The measured equivalence of this graph is depicted in Fig. 12.

remaining image. The physical information we acquire with this kind of ''atomic resolution'' is restricted to the value of one parameter: the maximum amount the AFM tip can be displaced from its relaxed position.

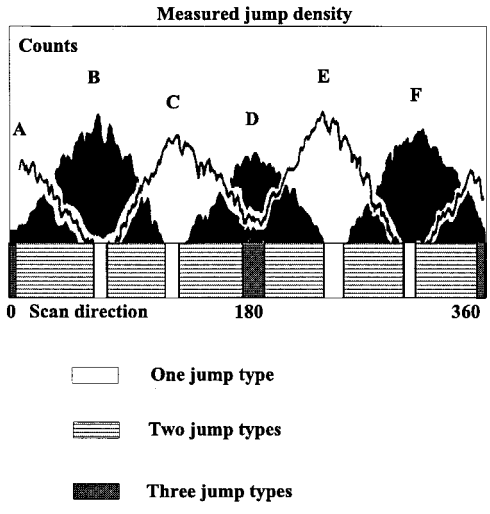

FIG. 12. Jump density curves (see also Fig. 11) as measured from the cluster shift contour plot in Fig. 10. Regions of one-, two-, and three-jump types occurring simultaneously can be distinguished. This effect is due to cantilever stiffness anisotropy which influences the maximum displacement of the stick tip. The transitions from one region to another can be used to calculate this maximum displacement.

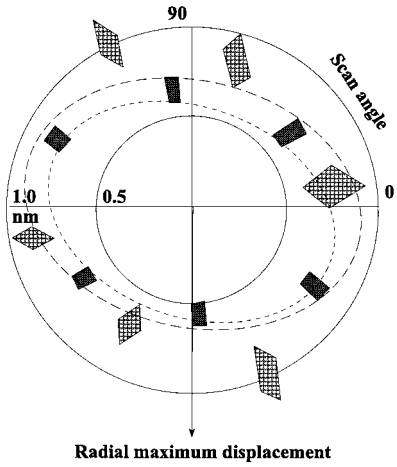

FIG. 13. A polar graph of the maximum displacement values, measured from two independent image characteristics. Open diamonds: calculated from the measured jumping behavior. Closed bars: calculated from the measured initial sticking. We see a rough correspondence, with the jump values some 20% larger than the sticking values and some misalignment of the anisotropy in each case.

ACKNOWLEDGMENTS

This work is part of the research program of the Foundation for Fundamental Research on Matter (FOM-Utrecht) and has been made possible by financial support from the Netherlands Foundation for Technical Sciences (STW-Utrecht).

APPENDIX A: CONSTRUCTION AND DERIVATION OF MODEL VALIDITY AND JUMP DENSITIES

Validity

See Fig. 14. When ϵ_0 becomes too small relative to the lattice distance λ, jump situations exist that may result in a larger displacement ϵ than before the jump took place. This is physically not reasonable. In practice, the cantilever tip would come to rest in its free relaxed state, which state is not accounted for in our model. From Fig. 14, this happens when $\epsilon_0 \leqslant \lambda/\sqrt{3}$.

Transition from a two- to a three-jump types situation

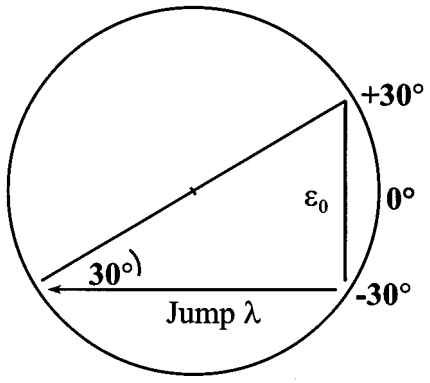

FIG. 14. Construction with minimal displacement circle. A smaller radius would result in nonrelaxing jumps.

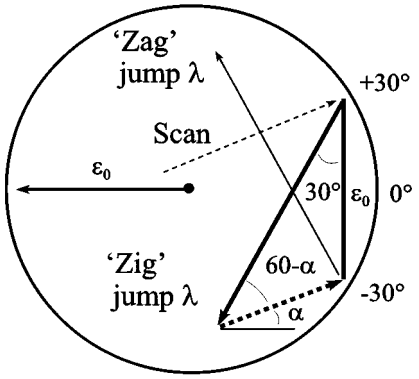

FIG. 15. Construction with only one possible ''zig''-''zag'' jump sequence. This situation couples the maximum displacement circle to the scan angle and the lattice distance lambda.

In Fig. 15, a situation is constructed in which only one possibility exists for a zig-zag jump sequence. The ''zig'' jump starting at 30° brings the tip position at the lowest ϵ_y. If α is such that the subsequent scan route crosses the maximum strain circle just below $-30°$, in the ''zag'' jump sector, a zag jump will follow. The sine rule gives:

$$\frac{\sin(60-\alpha)}{\epsilon_0}=\frac{\sin(90+\alpha)}{\lambda}, \tag{A1}$$

and this results in Eqs. (1), (3), and (5):

$$\alpha_{\text{zigzag}}=\arctan(\sqrt{3}-2\epsilon_0/\lambda). \tag{A2}$$

Jump density

When the angle α becomes larger or ϵ_0 becomes smaller, no ''zag'' jumps can occur any more. If this is the case, a long line scan l must be solely composed of (n_{zig}) ''zig'' type jumps and (n_{straight}) ''straight'' type jumps:

$$n_{\text{zig}}\begin{pmatrix}\lambda/2\\ \sqrt{3}\lambda/2\end{pmatrix}+n_{\text{straight}}\begin{pmatrix}\lambda\\ 0\end{pmatrix}=l\begin{pmatrix}\cos(\alpha)\\ \sin(\alpha)\end{pmatrix}. \tag{A3}$$

The normalized densities are $\rho_{\text{zig}}\equiv n_{\text{zig}}/n_{\text{zig}}+n_{\text{straight}}$ and $\rho_{\text{straight}}\equiv n_{\text{straight}}/n_{\text{zig}}+n_{\text{straight}}$.

TABLE I. Calculated jump densities.

	$\epsilon_0=\frac{\sqrt{3}}{3}$	$\epsilon_0=\frac{\sqrt{3}}{2}$
0°	$\rho_{\text{zig}}=0.25$	$\rho_{\text{zig}}=0$
	$\rho_{\text{straight}}=0.5$	$\rho_{\text{straight}}=1$
	$\rho_{\text{zag}}=0.25$	$\rho_{\text{zag}}=0$
30°	$\rho_{\text{zig}}=0.5$	$\rho_{\text{zig}}=0.5$
	$\rho_{\text{straight}}=0.5$	$\rho_{\text{straight}}=0.5$
	$\rho_{\text{zag}}=0$	$\rho_{\text{zag}}=0$

Using Eq. (A3) this results in Eqs. (A4a) and (A4b):

$$\rho_{\text{zig}}=\frac{2}{\sqrt{3}/\tan(\alpha)+1} \tag{A4a}$$

$$\rho_{\text{straight}}=\frac{\sqrt{3}/\tan(\alpha)-1}{\sqrt{3}/\tan(\alpha)+1} \tag{A4b}$$

In Fig. 16, we see a case in which α is larger or ϵ_0 is smaller than in Eq. (A2). Now there exist repeated series of zig-zag jump sequences, alternated with series of straight jumps sequences. Only the relevant construction lines are shown. Let the number of scan lines per area scanned being constant, the number of circle crossings will be proportional to $\{d_{\text{zig}},d_{\text{straight}},d_{\text{zag}}\}$, i.e., the number of jumps of type i, n_i:

$$n_i=C.d_i. \tag{A5}$$

For the ''straight'' jump type in sector $[-30°, +30°]$, Eq. (A5) becomes (see Fig. 16)

$$n_{\text{straight}}=C.\epsilon_0.\cos(\alpha). \tag{A6}$$

For the ''zag'' jump type in sector $[<-30°]$, Eq. (A5) becomes:

$$n_{\text{zag}}=C.\Delta_1.\sin(60-\alpha). \tag{A7}$$

For the line piece with length $(\lambda-\Delta_1)$ Eq. (A2) still holds with λ replaced by $\lambda-\Delta_1$:

$$\alpha=\arctan[\sqrt{3}-2\epsilon_0/(\lambda-\Delta_1)]. \tag{A8}$$

This, combined with (A7) leads to

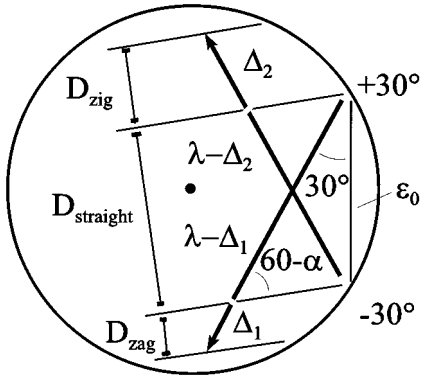

FIG. 16. The general construction situation with all three ''zig'', ''zag'', and ''straight'' jump types incorporated. The line pieces D have a length proportional to the corresponding relative abundance of each of the jump types.

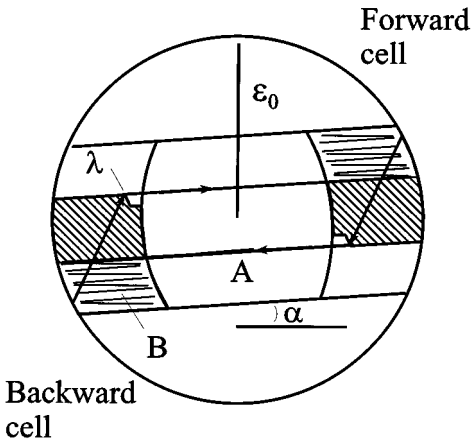

FIG. 17. Construction depicting the turnaround scan behavior of the tip. The contours of the periodic forward and backward cell are shaded. The distance that needs to be scanned for the first ''zig'' jump to occur in the backward cell is given by the line pieces labeled A and B.

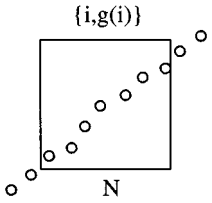

FIG. 18. Linear regression on a collection of N pixels with their values.

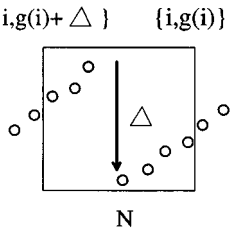

FIG. 19. Inserting a step in a more or less linear ramp.

$$n_{\mathrm{zag}}=C.[\lambda/2(\sqrt{3}\cos(\alpha)-\sin(\alpha))-\epsilon_0\cos(\alpha)]. \quad \text{(A9)}$$

For the last jump type, ''zig'' in the sector $[>+30]$, we have for Eq. (A5) (see Fig. 16):

$$n_{\mathrm{zig}}=C.\Delta_2.\sin(60+\alpha). \quad \text{(A10)}$$

We can eliminate Δ_2 from this with a sine rule relation in Fig. 15:

$$\frac{\lambda-\Delta_2}{\sin(90-\alpha)}=\frac{\epsilon_0}{\sin(60+\alpha)}. \quad \text{(A11)}$$

Then n_{zig} finally results in

$$n_{\mathrm{zig}}=C.[\lambda/2(\sqrt{3}\cos(\alpha)+\sin(\alpha))-\epsilon_0\cos(\alpha)]. \quad \text{(A12)}$$

Similar to the two jump type case, we can normalize the n_i on their sum from Eqs. (A6), (A9), (A12), to get the respective densities:

$$\Sigma_i n_i=C.(\lambda\sqrt{3}\cos(\alpha)-\epsilon_0\cos(\alpha)). \quad \text{(A13)}$$

Finally, with $\rho_i=n_i/\Sigma_i n_i$, this results in the three jump types situation as given in Eq. (2):

$$\rho_{\mathrm{zig}}=1-\frac{1}{2}\left(\frac{1-\tan(\alpha)/\sqrt{3}}{1-\epsilon_0/\lambda\sqrt{3}}\right), \quad \text{(A14a)}$$

$$\rho_{\mathrm{straight}}=\frac{1}{\lambda\sqrt{3}/\epsilon_0-1}, \quad \text{(A14b)}$$

$$\rho_{\mathrm{zag}}=1-\frac{1}{2}\left(\frac{1+\tan(\alpha)/\sqrt{3}}{1-\epsilon_0/\lambda\sqrt{3}}\right). \quad \text{(A14c)}$$

For two common scan directions, the influence of the maximum strain ϵ_0 on which type of jumps do occur was calculated from Eqs. (A13) and (A4). The results are given in Table I. The corresponding unit cell shapes can be seen in Fig. 3 of the main text.

In the one-jump type situation at every turn of a scan, labeled ''B'' in Fig. 17 in the backward cell, a certain distance of scanning is needed before the system is at the point in the reverse cell where the first side or ''zig'' jump will occur. The shortest possible route, which will happen once in a while, is shown. The first part ''A'' of this distance is the part to the first circle crossing. This distance is approximated by

$$A=\left(\sqrt{3}\epsilon_0-\frac{1}{2}\lambda\right)\Big/\cos(\alpha). \quad \text{(A15)}$$

For this, the circle is replaced by a line through plus and minus 30°. The maximum error is 8%, a value that corresponds, with scan sizes $>\sim 10\ \lambda$, to ca. 1% in the final result with the ''straight'' jump sequence added. The shaded part in Fig. 17 must be traveled by series of ''straight'' type jumps. With an approach similar to the calculation of the three-jump type density we find for this distance:

$$B=\epsilon_0\left(\frac{\cos^2(\alpha)}{\sin(\alpha)}-\sqrt{3}\cos(\alpha)\right)+\lambda\left(\frac{1}{2}\cos(\alpha)-\frac{1}{2}\sqrt{3}\frac{\cos^2(\alpha)}{\sin(\alpha)}\right). \quad \text{(A16)}$$

If the total distance $A+B$ from Eqs. (A15) and (A16) exceeds the scan size, no ''zig'' jumps will be observed. At the angle where this state changes to the periodic two-jump situation we have an equality $scansize=A+B$ and with Eqs. (A15) and (A16) we find from this for ϵ_0:

$$\epsilon_0=\frac{\mathrm{scansize}-\lambda\left[\left(\frac{1}{2}\right)\sqrt{3}\frac{\cos^2(\alpha)}{\sin(\alpha)}-\left(\frac{1}{2}\right)\cos(\alpha)+\frac{1}{2\cos(\alpha)}\right]}{\frac{\cos^2(\alpha)}{\sin(\alpha)}-\sqrt{3}\cos(\alpha)+\frac{\sqrt{3}}{\cos(\alpha)}}, \quad \text{(A17)}$$

where $\alpha=\alpha_{\mathrm{zig}}$.

At scan sizes $>10\ \lambda$, which is needed to get enough jump events experimentally, and $\alpha<15°$, we can simplify this expression with an accuracy of 2% to Eq. (8):

$$\epsilon_0=\mathrm{scansize}\,\frac{\alpha_{\mathrm{zig}}}{60}+0.87\lambda. \quad \text{(A18)}$$

Initial sticking

At every turn of a scan, the tip needs to be displaced a certain distance to make its first backward jump. This distance is angle and position dependent. We only consider the shortest possible routes ''C'' and ''D'' at zero and 30° scan direction. Both occur when the turning takes place directly after a ''straight'' jump in the forward cell. By construction we easily find

$$C=\sqrt{3}\epsilon_0-\lambda \quad \text{(A19a)}$$

at $\alpha=0$, and

$$D=\epsilon_0-\frac{1}{2}\sqrt{3}\lambda+\sqrt{\epsilon_0^2-\frac{1}{4}\lambda^2} \quad \text{(A19b)}$$

at $\alpha=30$. ''*D*'' is somewhat larger than ''*C*,'' with a maximum of 0.27 ϵ_0 for $\lambda=0$. At all other angles this shortest distance is in between.

APPENDIX B: LINEAR REGRESSION ON STICK-SLIP SIGNALS

A common characteristic of any stick-slip signal is the alternating of linear parts with steps of fixed amplitude. To distinguish between these two events, we use the linear regression routine. In. Fig. 18, we take N pixel-value pairs $\{i,g(i)\}$ with i from 1 to N. The slope of their best linear fit is:

$$\text{Slope}=\frac{\Sigma g(i)}{\Sigma i}-\frac{N}{\Sigma i}.\frac{\Sigma i.\Sigma ig(i)-\Sigma i^2.\Sigma g(i)}{\Sigma i.\Sigma i-N\Sigma i^2}, \tag{B1}$$

where each summation runs from 1 to N. In Fig. 19 we take the same group of pixels, but have inserted a step of height Δ at the point i_Δ:

$$\{i,g(i)\}\rightarrow \quad \{i,g(i)+\Delta\} \quad \text{for} \quad 1\leqslant i\leqslant i_\Delta \quad \text{and}$$
$$\{i,g(i)\} \quad \text{for} \quad i_\Delta<i\leqslant N.$$

This changes the sum terms in Eq. (B1):

$$\Sigma ig(i)\rightarrow\Sigma ig(i)+\Delta.\Sigma i \quad \Leftrightarrow$$
$$\Sigma i.g(i)\rightarrow\Sigma i.g(i)+\frac{1}{2}.\Delta.i_\Delta(i_\Delta+1) \tag{B2}$$

and

$$\Sigma g(i)\rightarrow\Sigma g(i)+\Delta.i_\Delta. \tag{B3}$$

Inserting Eqs. (B2) and (B3) into Eq. (B1) we obtain:

$$\text{Slope}_\Delta=\frac{\Sigma g(i)}{\Sigma i}+\frac{\Delta.i_\Delta}{\Sigma i}-\frac{N}{\Sigma i}.\frac{\Sigma i(\Sigma i.g(i)+1/2\Delta.i_\Delta.(i_\Delta+1))-\Sigma i^2(\Sigma g(i)+\Delta.i_\Delta)}{\Sigma i\Sigma i-N\Sigma i^2}$$

with the help of (B1) the original slope can be extracted, resulting in:

$$\text{Slope}_\Delta=\text{Slope}+\Delta.i_\Delta.\frac{2(N-i_\Delta)}{N.(N+1)^2-4\Sigma i^2}. \tag{B4}$$

If such a step Δ is encountered a large number of times, we may replace

$$\frac{i_\Delta}{N}\rightarrow x, \quad \text{with} \quad x\in(0,1),$$

which results in:

$$\text{Shift}=\text{Slope}_\Delta-\text{Slope}=F(N)x(1-x)\Delta, \tag{B5}$$

where $F(N)=[2N^2/N.(1+N)^2-4\Sigma i^2]$. The maximum shift in slope after linear regression on a step is proportional to its height. For $N>8$, $F(N)$ can be approximated within 1% by $6/N$. Applying this to Eq. (B5) results in Eq. (12) of the main text, namely:

$$\text{Shift}=\Delta.\frac{6}{N}.x(1-x). \tag{B6}$$

The maximum shift is for $x=i/N=1/2$ and as a result follows Eq. (13):

$$\text{Shift}=\frac{3\Delta}{2N}. \tag{B7}$$

[1] S. J. O'Shea, M. E. Welland, and T. M. H. Wong, Ultramicroscopy **52**, 55 (1993).

[2] S. Grafstrom, J. Ackermann, T. Hagen, R. Neumann, O. Probst, J. Vac. Sci. Technol. B **12**, 1559 1994.

[3] R. J. Warmack, X. -Y. Zheng, T. Thundat, and D. P. Allison, Rev. Sci. Instrum. **65**, 394 (1994).

[4] S. Fujisawa, E. Kishi, Y. Sugawara, and S. Morita, Jpn. J. Appl. Phys. **33**, 3752 (1994).

[5] S. Fujisawa, M. Ohta, T. Konishi, Y. Sugawara, and S. Morita, Rev. Sci. Instrum. **65**, 644 (1994).

[6] O. Marti, J. Colchero, and J. Mlynek, Nanotechnology **1**, 141 (1990).

[7] J.-A. Ruan and B. Bhushan, J. Appl. Phys. **76**, 5022 (1994).

[8] C. M. Mate, G. M. McClelland, R. Erlandsson, and S. Chiang, Phys. Rev. Lett. **59**, 1942 (1987).

[9] R. Erlandsson, G. Hadziioannou, C. M. Mata, G. M. McClelland, and S. Chiang, J. Chem. Phys. **89**, 5190 (1988).

[10] D. Tomanek, W. Zhong, and H. Thomas, Europhys. Lett. **15**, 887 (1991).

[11] H. Heinzelmann, E. Meyer, D. Brodbeck, G. Overney, and H.-J. Guntherodt, Z. Phys. B Condens. Matter **88**, 321 (1992).

[12] S. Fujisawa, Y. Sugawara, S. Ito, S. Mishima, T. Okada, and S. Morita, Nanotechnology **4**, 138 (1993).

[13] R. M. Overney, H. Takanoan, M. Fujihira, W. Paulus, and H. Ringsdorf, Phys. Rev. Lett. **72**, 3546 (1994).

[14] I. L. Singer, J. Vac. Sci. Technol. A **12**, xxx (1994)

[15] J. Kerssemakers and J. Th. M. De Hosson, Appl. Phys. Lett. **67**, 347 (1995).

[16] J. Grasman, *Asymptotic Methods for Relaxation Oscillations and Applications,* Applied Mathematical Sciences (Springer-Verlag, New York, 1987).

[17] S. Fujisawa, Y. Sugawara, S. Morita, S. Ito, S. Mishima, and T. Tokada, J. Vac. Sci. Technol. B **12**, 1635 (1994).

[18] H. Kawakatsu, T. Saito, H. Kougami, P. Blanalt, M. Kawai, M. Watanabe, and N. Nishioki J. Vac. Sci. Technol. B **12**, 1686 (1994).

[19] M. Labardi, M. Allegrini, M. Salerno, C. Frediani, and C. Ascoli, Appl. Phys. A **59**, 3 (1994).

[20] J. M. Neumeister and W. A. Ducker, Rev. Sci. Instrum. **65**, 2527 (1994).